Biomaterials 241 (2020) 119880

Contents lists available at ScienceDirect

Biomaterials

journal homepage: www.elsevier.com/locate/biomaterials

Multifunctional synthetic Bowman's membrane-stromal biomimetic for corneal reconstruction

Xiaokun Wang[a,1], Shoumyo Majumdar[a,1], Uri Soiberman[b], Joshua N. Webb[c], Liam Chung[a], Giuliano Scarcelli[c], Jennifer H. Elisseeff[a,*]

[a] Translational Tissue Engineering Center, Wilmer Eye Institute, Johns Hopkins School of Medicine, Baltimore, MD, USA
[b] Department of Ophthalmology, Johns Hopkins Hospital, Baltimore, MD, USA
[c] A. James Clark School of Bioengineering, University of Maryland, College Park, MD, USA

ARTICLE INFO

Keywords:
Collagen vitrigel
Biomimetic
Corneal transplantation
Reepithelialization
Stromal regeneration

ABSTRACT

As the outermost layer of the eye, the cornea is vulnerable to physical and chemical trauma, which can result in loss of transparency and lead to corneal blindness. Given the global corneal donor shortage, there is an unmet need for biocompatible corneal substitutes that have high transparency, mechanical integrity and regenerative potentials. Herein we engineered a dual-layered collagen vitrigel containing biomimetic synthetic Bowman's membrane (sBM) and stromal layer (sSL). The sBM supported rapid epithelial cell migration, maturation and multilayer formation, and the sSL containing tissue-derived extracellular matrix (ECM) microparticles presented a biomimetic lamellar ultrastructure mimicking the native corneal stroma. The incorporation of tissue-derived microparticles in sSL layer significantly enhanced the mechanical properties and suturability of the implant without compromising the transparency after vitrification. *In vivo* performance of the vitrigel in a rabbit anterior lamellar keratoplasty model showed full re-epithelialization within 14 days and integration of the vitrigel with the host tissue stroma by day 30. The migrated epithelial cells formed functional multilayer with limbal stem cell marker p63 K14 expressed in the lower layer, epithelial marker K3 and K12 expressed through the layers and tight junction protein ZO-1 expressed by the multilayers. Corneal fibroblasts migrated into the implants to facilitate host/implant integration and corneal stromal regeneration. In summary, these results suggest that the multi-functional layers of this novel collagen vitrigel exhibited significantly improved biological performance as corneal substitute by harnessing a fast re-epithelialization and stromal regeneration potential.

1. Introduction

Vision loss due to corneal disease or trauma is a leading cause of blindness worldwide and the burden varies by region [1]. Keratoplasty is considered the best option to restore vision in patients who suffer from corneal blindness. Several barriers hinder the effectiveness of keratoplasty, such as limited availability of transplant tissue and transplant rejections. Globally, around 10 million individuals are blind due to corneal damage or disease and only less than 1% of the global need for donor cornea tissue is being met [2]. Therefore, alternative solutions to substitute donor tissues are in high demand.

Several strategies have been employed to replace donor corneal tissues. Purely synthetic materials, such as poly(methyl methacrylate), are utilized as corneal substitutes for patients with multiple donor cornea rejections [3]. However, these synthetic materials do not allow host-implant integration, leading to a high failure rate with inflammation and implant extrusion [4]. According to clinical reports, only half of the eyes retained their initial keratoprosthesis during the follow up [5]. Biological and biosynthetic materials, such as silk and crosslinked collagen, are also used for corneal substitutes [6,7]. These crosslinked hydrogels presented high optical transparency and early clinical trials demonstrated biocompatibility in patients [8]. Unfortunately, overlay sutures are routinely used on such implants instead of standard interrupted sutures due to limited mechanical integrity caused by crosslinking [9]. These materials do not have the unique fibril arrangement of collagen lamellae that is in the corneal stroma that provides robust mechanical strength.

Material scientists are working to recreate the complex lamellar structure of the cornea in biomaterial substitutes. For example, structured implants were engineered using corneal fibroblasts in a layer-by-

* Corresponding author. Translational Tissue Engineering Center, Wilmer Eye Institute, Johns Hopkins School of Medicine, Baltimore, MD, USA.
E-mail address: jhe@jhu.edu (J.H. Elisseeff).
[1] Contributed equally.

https://doi.org/10.1016/j.biomaterials.2020.119880
Received 8 October 2019; Received in revised form 23 January 2020; Accepted 10 February 2020
Available online 14 February 2020
0142-9612/

layer manner with different substrates such as gelatin [10], collagen film [11], silk fibrins [12], and peptide amphiphile [13]. The corneal fibroblasts secrete stromal extracellular matrix within the biomaterial scaffold to engineer a corneal stromal equivalent [14]. These engineered corneal equivalents with corneal fibroblasts achieve structural similarity to the native cornea; however, they are not clinically practical due to limited thickness and relatively complicated process of such corneal equivalents. Another solution is to use pure material-based approaches to recreate the lamellar structure that utilize the self-assembly nature of fibrillar collagen such as molecular crowding [15] and long-term dialysis [16]. Although various *in vitro* studies showed that corneal epithelial cells were able to grow on collagen membrane using molecular crowding technique [17], they lacked follow up studies to investigate how those cells performed *in vivo*. In our previous studies, we developed corneal stroma-mimetic biomaterials via vitrification, a controlled dehydration process which facilitated a gradually increase in the concentration of collagen and assembly. This product, named "vitrigels", could be used for variety of ocular applications [18]. Cyclodextrins (CD) added to the collagen and vitrification process further modulated to resemble the structure of native corneal stroma [19]. The resulting collagen vitrigel exhibits similar lamellae structures to native corneal stroma, and this unique ultrastructure allows the collagen vitrigel for high optical transparency and robust mechanical integrity that are essential for *in vivo* implantation with simple interrupted sutures.

Besides the requirements for key physical properties such as high optical transparency and mechanical integrity, re-epithelialization efficiency and biocompatible integration with the host are also critical for all synthetic corneal substitutes. In the native human cornea, a non-lamellar, Bowman's layer lies in between the corneal stroma and epithelium. Quick re-epithelialization is critical to prevent infection and to encourage implant/host integration [20]. Previously described *in vitro* studies have demonstrated that biomaterial mechanics and surface roughness influence epithelial cell migration and maturation [21,22]. To address the challenge of re-epithelialization, we incorporated a thin, ultrastructurally homogenous Bowman's layer-like biosynthetic membrane on top of the synthetic corneal stromal layer, to create a dual-layered corneal substitute.

Integration of corneal implants of any type remains a significant barrier to clinical success. Acellular extracellular matrix (ECM) derived from biological tissues holds a great biological and regenerative potential. The ECM of amniotic membrane had been used for ocular surface reconstruction in the clinic for decades [23,24]. While highly compatible, physical properties are limited and degradation is fast. ECM biomaterials have been applied clinically in many forms, such as loose particles [25], sheet [26], or 3D supporting scaffolds [26] to promote wound healing and regeneration. Although the use of ECM in ocular tissue engineering is not as common as other organs, ECM particles had been implicated in corneal stromal wound and significantly reduced corneal scarring [27]. Here, we combined porcine small intestinal submucosa (SIS)-derived ECM into the synthetic stromal layer, in order to promote the biological performance of the corneal implant.

Here, we present a dual-layered corneal substitute consisting of a synthetic Bowman's membrane (sBM) and a synthetic stromal layer (sSL). While the sBM supports a rapid re-epithelialization, the sSL improves the mechanical and biological compatibility of the implant. The sBM layer was engineered as a thin, homogenous, non-lamellar collagen layer to mimic the basement membrane. The sSL was made from beta cyclodextrin (βCD)-mediated collagen vitrigel as previously described [19], and comprised the majority thickness of the bioengineered corneal subsitiute. In addition, SIS ECM microparticles were added to the sSL to further enhance the mechanical properties and biocompatibility. The dual-layered corneal substitute was engineered to support rapid re-epithelialization as well as maintain transparency, mechanical strength and allow host/implant integration *in vivo*.

2. Materials and methods

2.1. Preparation of dual-layered corneal substitute materials

Corneal substitutes were engineered as follows. The sBM gel was created by using 1.5 mL of 5 mg/ml type I collagen solution (Cosmo Bio KOU-IPC-50, Atelocollagen from Bovine dermis) each in 6-well tissue culture plates and placed in an ammonium vapor environment for 5 min. The sSL layer was prepared immediately following sBM gelation and 5 mL of sSL mixture was poured over the sBM gel. The sSL layer was prepared at 4 °C by mixing equal volumes of 5 mg/ml type I collagen solution and a neutralization mixture consisting 2.5 mg/ml beta cyclodextric (βCD) (Sigma Aldrich, St. Louis, MO) solution, 20 mM HEPES (Life Technologies) and 5 mg/ml of porcine small intestine submucosa (SIS) matrix microparticles passed through a 40 μm filter, at pH 11. The SIS matrix was prepared as described in a previous publication [28]. The solution contained SIS microparticles were filtered through 40 μm cell strainer three times before mixing with the collagen. The resulting combination gel was then placed in a sterile controlled humidity chamber (vitrifier) at 5 °C and 40% relative humidity (RH) for 1 day, and then further dehydrated in a second vitrifier at 40 °C and 40% RH for 1 week to form transparent, rigid vitrigel materials. Vitrigel materials were rehydrated in 20 mM HEPES buffer for 1 h before use.

2.2. Second harmonic generation (SHG) microscopy

Hydrated materials were used for SHG microscopy imaging. Samples were placed on a glass slide with cover slip and examined using a Zeiss LSM 710 microscope (Zeiss, Oberkochen, Germany) with a 790 nm excitation wavelength, 20× objective and scanning speed of 7. The image sections were captured at 5 μm increments across a scanning depth of 400 μm. The 3D reconstruction of the SHG image for each sample was performed using the software ZEN (Zeiss, Oberkochen, Germany).

2.3. Electron microscopy

Samples were first fixed using 0.1 M sodium cacodylate buffer with 3% paraformaldehyde (PFA), 1.5% glutaraldehyde, 2.5% sucrose, and 0.1% tannic acid, followed by post-fixation in osmium tetroxide. Aqueous uranyl acetate was used to accentuate collagen fibril staining in all samples. Following dehydration using a graded series of ethanol, samples were ready for electron microscopy. For Transmission electron microscopy, samples were embedded in Eponate 12 resin (Ted Pella, Redding, CA). Thin sections, 60–90 nm were placed on naked copper grids. Transmission electron microscope (TEM) images were taken by CM120 TEM (Philips, Amsterdam, Netherlands) at 80 kV. Scanning electron microscopy (SEM) samples were fixed as described above and affixed to SEM stubs, coated with 20 nm AuPd, and observed using a Leo FESEM (Zeiss, Oberkochen, Germany). Lamellar thickness was determined using ImageJ software (NIH, Bethesda, MD).

2.4. Light transmittance

Fully hydrated materials were placed flat on 24-well plates. Light absorbance was measured using the area scanning modality on a Biotek Synergy 2 microplate reader in the visible light wavelength range of 300–700 nm with 50 nm intervals. Absorbance values were converted to light transmittance values using the Beer-Lambert law.

2.5. Tensile testing and suturability

Hydrated materials were cut into 5 mm width test strips, secured with superglue and sandpaper grips. Control native corneal strips were obtained from fresh rabbit eyes purchased from PelFreez (PelFreez Biologicals, Rogers, AR). Sample thickness was measured using digital

Vernier calipers (Mitutoyo, Japan). Samples were loaded onto a Criterion 43 Tensile Tester (MTS, Eden Prairie, MN) with a 100 N load cell and stretched uniaxially at a speed of 0.02 mm/s until failure, with an initial test sample length of 1 cm. Load vs displacement values were recorded and analyzed.

The suturability set up was shown in our previous publication [29] and Supplemental Fig. 1A. A 10-0 nylon suture ran through the material and was loaded onto Criterion 43 Tensile Tester (MTS, Eden Prairie, MN) with a 250 g load cell and stretched at a speed of 0.02 mm/s until failure. Load values were recorded and analyzed.

2.6. Degradability

The degradability was tested by digesting native corneas, sBM and sSL materials in collagenase type II. In brief, all samples were stored in PBS for 24 h prior to the test, and degradation was carried out by soaking samples in 100 U collagenase type II (Sigma Aldrich). At each time point, the excess water was removed by kimwipes and the weight was recorded.

2.7. Ex vivo corneal epithelial cell migration

Fresh rabbit eyes were purchased from PelFreez (PelFreez Biologicals, Rogers, AR). Implants of 6 mm diameter were surgically inserted into *ex vivo* corneas after creation of a partial pocket model with a 4 mm anterior wound (Fig. 4a). The corneas with the implants were placed on convex molds matched to corneal curvature. The *ex vivo* corneas were then air-lift cultured in full media (DMEM + 10% fetal bovine serum) for up to 72 h. Re-epithelialization was tracked using Fluoresoft (Alden Optical, Lancaster, NY) solution, with a blue light source. Briefly, one drop of Fluoresoft solution was applied to the *ex vivo* corneal surface, following by extensive rinsing with PBS. Blue LED light source was used to observe the fluorescein staining. Following the 72 h time point, samples from the same test group were chosen at random for either paraffin embedding or for immunofluorescent staining. Samples for paraffin embedding were fixed in 10% formalin, dehydrated, embedded in paraffin, sectioned using a microtome and stained using hematoxylin and eosin according to standard protocol. Samples for immunofluorescent staining were carefully removed from the corneal pockets and fixed in 4% PFA followed by immunofluorescent staining for ZO-1 and K14.

2.8. Isolation and culture of corneal fibroblasts

Corneal fibroblasts were isolated from fresh rabbit eyes (PelFreez Biologicals, Rogers, AR). Excised corneas were incubated overnight at 4 °C in 1 mg/ml of Dispase II (Roche) in PBS (Thermo Fisher). The loosened epithelial sheets were gently scraped off and discarded. Each corneal stroma was further cut into smaller pieces and further digested using 2 mg/ml collagenase type II for 2 h at 37 °C with mechanical agitation. The digested cells were filtered through a 70 μm cell strainer to remove extracellular debris. The primary corneal fibroblast cell suspension was appropriately diluted and seeded on sBM and sSL substrates at 5000 cells/cm^2 seeding density in full medium (DMEM + 10% fetal bovine serum). Cells on various substrates were confluent by day 5. Certain wells of keratocytes growing on various substrates were chosen at random and stimulated using 20 ng/ml pro-inflammatory cytokine IL-1β (Thermo Fisher Scientific) in complete medium, following confluence. Cells were cultured in IL-1β containing media for 24 h before harvest for gene expression studies.

2.9. Quantitative real tme polymerase chain reaction (qRT-PCR)

Corneal fibroblasts were harvested for qRT-PCR at confluence. In brief, corneal fibroblast layers were washed with PBS 3 times, lysed with 500 μl Trizol (Thermo Fisher, Waltham Scientific, MA), and processed for standard RNA isolation. The mRNA was purified using RNeasy mini kit (Qiagen, Hilden, Germany), quantified by Nanodrop 2000 (Thermo Fisher Scientific, Waltham, MA), and reverse transcribed using a High Capacity cDNA reverse transcription kit (Thermo Fisher, Waltham, MA). Gene expression was characterized by qPCR with SYBR green master mix (Thermo Fisher Scientific, Waltham, MA). GAPDH was used as internal control, and the relative expression of genes was quantified using $2^{-\Delta\Delta Ct}$. The primer sequences (Table 1) were designed using Primer-BLAST (NCBI, https://www.ncbi.nlm.nih.gov/tools/primer-blast/).

Table 1
Primer sequences for qPCR.

Gene	Sequence
GAPDH	Forward: CTCTGGAGTGGATGTT Reverse: CCATGGGTGGAATCATACTG
Keratocan (KERA)	Forward: AGTACCAACAAGCTTCAGCC Reverse: ACCCAGATGACGAAACATATT
ALDH	Forward: GACGATAACTGCAGAGCACG Reverse: ACTCATTCGACAAGCAGACAG
Biglycan	Forward: GCATCCCCAAAGATCTGCC Reverse: CAACTTGGAGTATCGGAGCAG
IL6	Forward: GAATAATGAGACCTGCCTGCT Reverse: TTCTTCGTCACTCCTGAACTTG
IL8	Forward: TGGACCTCACTGTGCAAA T Reverse: GCTCAGCCCTCTTCAAGAAT
MMP9	Forward: AGTACCGAGAGAAAGCCTACTT Reverse: TGCAGGATGTCAAAGCTCAC

2.10. Animal anterior lamellar keratoplasty

All the experimental procedures on animals in this study were performed in accordance to the Association for Research in Vision and Ophthalmology Statement for the Use of Animals in Ophthalmic and Visual Research, and were performed following approval from the Institutional Animal Care and Use Committee at Johns Hopkins University. Only one eye in each animal received surgery. Six male New Zealand albino rabbits (weight 2.5–3.5 kg) (5 received implant and 1 as negative control that did not receive implant) were anesthetized using intramuscular administration of ketamine (35 mg/kg) and xylazine (5 mg/kg). Proparacaine (Akorn, Lake Forest, IL) was administered on the corneal surface prior to the anterior lamellar keratectomy surgical procedure. A Hessburg-Barron vacuum trephine with 6 mm diameter (Barron Precision Instruments LLC, Grand Blanc, MI) and crescent knife (LaserEdge, Bausch & Lomb, Rochester, NY) were used to surgically remove approximately 250 μm of corneal tissue. The dual-layered collagen vitrigel implants, approximately 250 μm in thickness and 6.5 mm in diameter were implanted into the wound bed. The material was fixed using 8 to 12 interrupted 10-0 nylon sutures. The animals were allowed to recover and PRED-G ointment (Allergan, Irvine, CA) was applied to the eyes twice daily for 14 days post-surgery. Gross observations, including ophthalmomicroscopy and fluorescein staining were performed at day 3, 7, 14, 21, and 30 days following surgery. Corneas were harvested at 30 days post-surgery, fixed in 10% formalin and processed for histology and immunostaining.

2.11. Histology and immunofluorescent staining

Following fixation in 10% Formalin, samples from *in vivo* and *ex vivo* experiments underwent standard graded dehydration procedure in ethanol, followed by xylene treatment. Following an overnight paraffin infiltration, each sample was oriented, embedded in paraffin wax and sectioned using a microtome (5 μm thickness). Slides were stained with Hematoxylin and Eosin and observed under bright field microscope (Zeiss). The corneal thickness at the center and peripherals was measured by ImageJ.

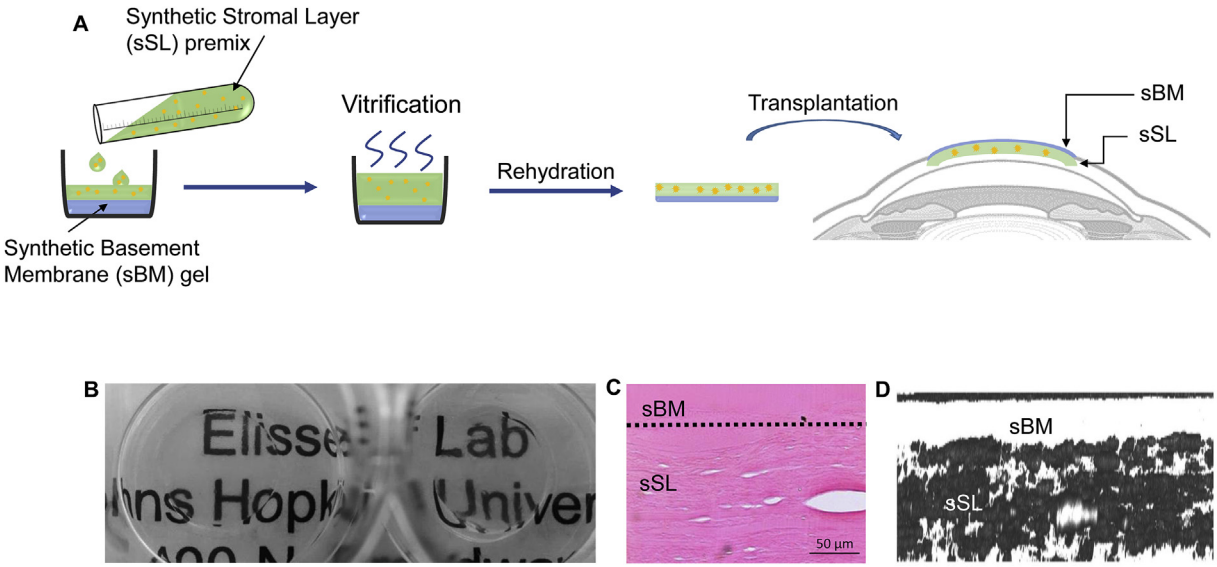

Fig. 1. Engineering the dual-layered collagen vitrigel corneal substitutes with synthetic basement membrane (sBM) and stromal layer (sSL). A) Schematic showing the manufacturing procedures of the dual-layered collagen vitrigel corneal substitutes. **B)** Gross photos demonstrating the high transparency of the dual-layered collagen vitrigel. Images of **C)** H&E staining and **D)** SHG of the cross-section of the collagen vitrigel presenting different ultrastructures of the sBM and sSL layers.

For immunofluorescent staining, slides were deparaffinized and the antigen retrieval was performed in citrate buffer (pH 6.0) for 20 min. Samples were treated with blocking buffer of PBS containing 1% BSA (bovine serum albumin) and 0.05% Triton-X for 30 min. For *ex vivo* samples, cytokeratin 14 (K-14) and zonula occludens 1 (ZO-1) (Chemicon, Temecula, CA)primary antibodies were stained at 1:100 concentration overnight at 4 ˚C, and for *in vivo* samples, K14, ZO-1, p63, K3, K12 (Chemicon), alpha smooth muscle actin (α-SMA) (Thermo Fisher Scientific), CD45 (Biolegend), Thy1 (Abcam) and integrin β4 (Abcam) were stained at concentration overnight at 4 ˚C, followed by secondary antibody staining (1:100 goat anti-rat Alexa Fluor 594, 647, Life Technologies) and counter stained with DAPI (Life Technologies).

2.12. Optical coherent tomography

The eyes of animals which underwent surgery were imaged with Envisu R4110 SDOCT system (Bioptigen, Durham, NC) with 10 mW output power light source, and an effective bandwidth of 105 nm centered at 845 nm. The transversal resolution is approximately 12 μm. The scanning area of each cornea had a width of 12 × 12 mm and depth of 1.2 mm.

2.13. Brillouin microscopy

Brillouin Microscopy was used to evaluate the spatially-resolved mechanical properties of the vitrigel samples. A confocal Brillouin microscope was utilized with similar configuration of previous studies (Scarcelli et al. Nat Methods 2015). Briefly, a 532 nm laser with an optical power of 10 mW was focused onto the sample by a 20X, 0.4 NA objective lens (Olympus America, Inc.) for a typical transverse resolution of 1 μm and depth resolution of 4 μm. The scattered light, collected through the same objective, was coupled into a single mode fiber and delivered to a two-stage VIPA spectrometer featuring an EMCCD camera (Andor, IXon Du-897) (Scarcelli and Yun, Opt. Express 2011). Each Brillouin spectrum was acquired in 0.2 s and fit using a Lorentzian function to quantify the Brillouin frequency shift at each point within the sample. The shift was calibrated using the known frequency shifts of water and glass.

The Brillouin frequency shift was related to the local mechanical properties by the following equation: $M' = \frac{\rho v_\beta^2 \lambda_i^2}{4n^2}$ in which M′ is the longitudinal elastic modulus, v_β is the measured Brillouin frequency shift, n is the refractive index of the material, λ_i is the wavelength of the incident photons, and ρ is the density of the material. The spatially varying ratio of $\frac{\rho}{n^2}$ was approximated to the constant value of 0.57 g/cm^3 based on literature values; we estimate this to introduce a 0.3% uncertainty throughout the cornea [30]. Previously, we have validated the strong relationship ($R > 0.9$) between Brillouin-derived modulus and the Young's Modulus found via gold-standard stress-strain compression tests on porcine corneas [31].

2.14. Statistical analysis

The light transmittance, tensile testing, and PCR analyses were performed with samples of $n = 5$, representative of two or more independent studies. Data are expressed as mean ± standard deviation. Statistical significance (p value) between conditions was determined by one-way analysis of variance (ANOVA) with Bonferroni post hoc test using GraphPad Prism 5. $P < 0.05$ is considered statistically significant.

3. Results

3.1. Dual-layered collagen vitrigel substitutes mimic physical properties of native corneas

To create a biosynthetic implant that resembles the cornea in both physical properties as well as re-epithelialization potential, we engineered the visually transparent, dual-layered corneal substitute (Fig. 1A) through a multi-step process. This combination product consisted of a sSL layer incorporated with tissue-derived microparticles, which provided the ultrastructural, optical and mechanical properties, and a sBM layer that improved the re-epithelialization. The vitrification procedure is a slow and controlled dehydration process that creates inter- and intra-molecular binding between collagen and ECM proteins [18,32], allowing the high-water content pre-vitrified hydrogel to form a transparent, strong, and high-collagen content vitrigel (Fig. 1B and C). The re-assembly of ECM-based materials using vitrification enables their application in the ocular environment.

The histological cross section of the dual-layered corneal substitute revealed a bilayered structure that included a homogenous sBM collagen layer transitioning smoothly into a lamellar sSL layer (Fig. 1C).

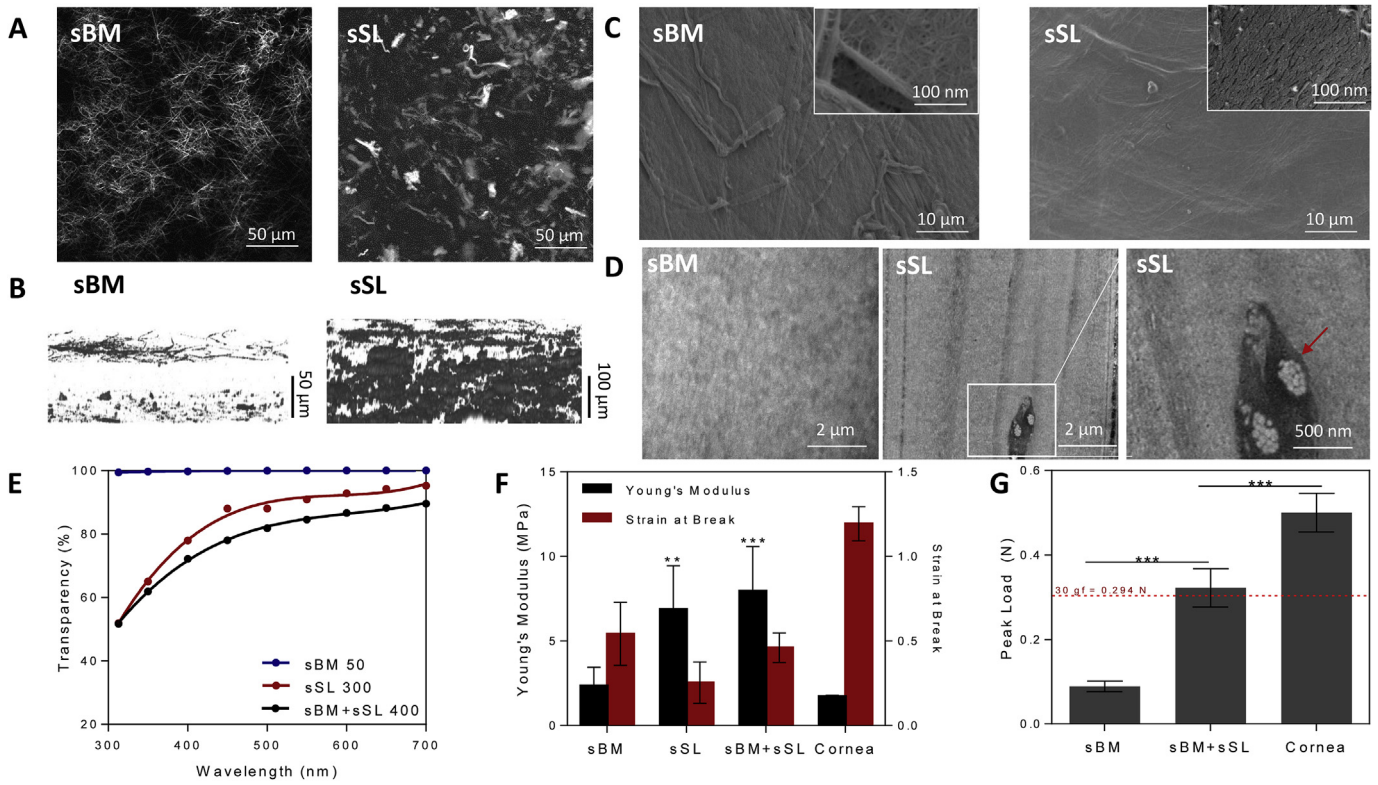

Fig. 2. Structural and physical properties of the dual-layered collagen vitrigel corneal substitutes. A) Horizontal view of the surface of sBM and sSL using SHG, collagen fibrils were visible in both layers of collagen materials **B)** Cross section view of sBM and sSL, showing collagen fibril structures were only visible on the air/gel and plate/gel interfaces of the sBM layer, while in the sSL layer, collagen fibril structures were visible throughout the entire material. **C)** SEM with low and high magnification, and **D)** TEM images of the sBM and sSL layers, demonstrating different ultrastructures of the two layers. **E)** Light transmittance of sBM layer of 50 μm, sSL layer of 300 μm, and the dual-layered collagen vitrigel of 400 μm transplantable thickness. **F)** Young's modulus and strain-at-break of the sBM material, sSL, the dual-layered material, and cornea control, n = 6 of each group of materials. (n = 5, *P < 0.05) **G)** The peak load of suturability test of materials of 400 μm.

SHG microscopy showed the collagen fibrillar organization, which confirmed an amorphous sBM layer and a fibrillar sSL (Fig. 1D). SHG scanning of independent sBM and sSL layers revealed collagen fibrils in sBM samples were visible only at the surface interfaces (air/gel and gel/plastic interface), while sSL membranes consisted of a fibrillar structure throughout (Fig. 2A and B). SEM imaging of sBM and sSL surfaces demonstrated scattered thick collagen fibrils and small porous collagen structures presented on the surface of sBM layers, while the surface of sSL layer presented densely packed aligned fibril structures (Fig. 2C). In addition, TEM images showed the ultrastructures of cross sections in sBM and sSL layers. The sBM cross section presented a homogenous collagen structures, while the sSL layer demonstrated a lamellar formation (Fig. 2D). In sSL layer, each lamella ranged between 500 nm and 2 μm in thickness. ECM microparticles in between the lamellae are visualized as the small dark spots. Notably, TEM images showed that ECM particles maintained small collagen bundles which indicated by the red arrow.

A high light transmission percentage in the visible light spectrum was essential for a corneal substitution material (Fig. 2E). Single layer of sBM or sSL, or the dual-layered corneal substitute were all tested for light transmission. The sBM layer, at 50 μm thickness, demonstrated nearly 100% transparent across all tested wavelengths. The sSL layer, at 300 μm thickness, presented over 80% light transmittance at the 550 nm (mid-range) visible light wavelength. The optical transparency of the 400 μm thick dual-layered collagen vitrigel showed over 75% light transmittance at 550 nm wavelength, indicating that the synthetized material was suitable in terms of transparency as a corneal substitute. Furthermore, the addition of ECM particles did not affect the transparency of the vitrigel, as the light transmittance values at 550 nm showed no significant difference between vitrigels with or without ECM particles (Supplemental Fig. 1B).

The mechanical properties of the dual-layered corneal substitute were characterized by tensile testing and suturability testing (Fig. 2F and G). The Young's modulus of the dual-layered collagen vitrigels was significantly higher than the native cornea. This high modulus was due to the nature of the sSL layer, which consisted of collagen, cyclodextrins, and ECM microparticles. The Young's modulus of the individual sBM layer was comparable to the native cornea (Fig. 2F). Since the Young's modulus values alone were not sufficient to provide information about suturability of the material, we performed more tests to investigate the suturability of the materials at 400 μm in thickness (Fig. 2G). The dual-layered collagen vitrigels were able to bear significantly higher load compared to sBM alone, demonstrating the importance of the sSL layer in enhancing mechanical strength. The incorporation of ECM microparticles within the sSL layer contributed to a significantly higher suture strength compared to ones without ECM microparticles (Supplemental Fig. 1C). Although incorporating ECM increased the suturability, the native cornea still had more robust integrity as compared to the biosynthetic corneal substitute (Fig. 2G). Degradation of the materials was assessed using the collagenase test (Supplemental Fig. 1D). The remaining ratio was calculated by ratio of the remaining weight divided by the original weight across multiple time points. No statistical difference was found between sSL and cornea group. The remaining ratio of sBM at 4 h and 18 h was significantly lower than cornea (*p < 0.05 Vs. Cornea).

Mechanical differences between two layers of the material were measured using Brillouin Microscopy (Supplemental Fig. 1E). As shown in the representative Brillouin map, the anterior section of the sample displayed lower Brillouin frequency shifts than the posterior. Therefore, based on the established relationship between Brillouin frequency shift

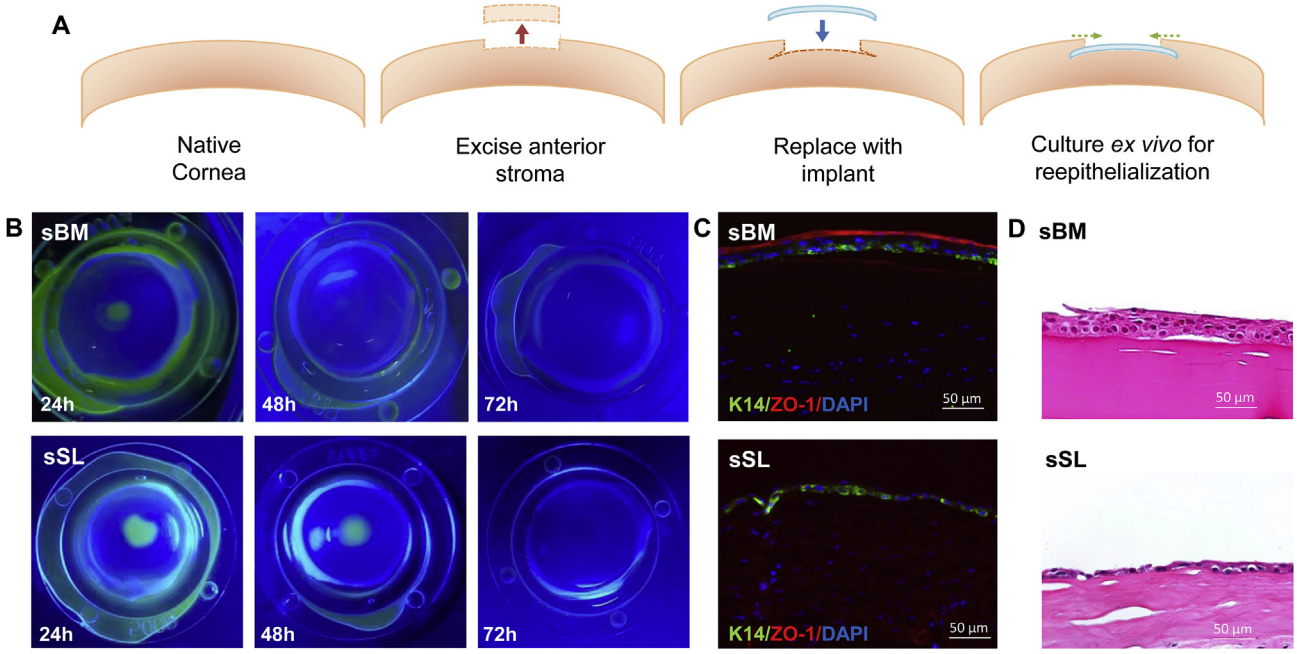

Fig. 3. Ex vivo re-epithelialization on sBM and sSL layer. A) Schematic showing the corneal organ culture model of *ex vivo* re-epithelialization. **B)** Fluorescein staining tracking the corneal epithelial cell migration within 72 h. **C)** immunofluorescent staining of corneal epithelial cell marker K14 (green), and tight junction formation ZO-1 (red) on sBM and sSL layers. **D)** H&E staining demonstrating epithelial cell multilayer formation on sBM layer and single layer formation on sSL layer. (For interpretation of the references to colour in this figure legend, the reader is referred to the Web version of this article.)

and mechanical properties, the anterior sSL layer was stiffer than the posterior sBM layer. Further, regions of increased tensile strength corresponding to the presence of dispersed ECM microparticles in the sSL layer were also observed as local areas of high Brillouin frequency shifts.

3.2. The synthetic basement membrane (sBM) promotes epithelial cell migration and maturation

We evaluated epithelial cell migration and maturation on sBM and sSL materials using an *ex vivo* whole corneal culture model (Fig. 3A). We tracked the epithelial cell migration over the materials using fluorescein staining. On sBM materials, epithelial cells migrated onto the 4 mm open wound and completely covered the sBM material within 48 h. On sSL materials, full reepithelialization was observed at 72 h (Fig. 3B) time point. Epithelial cell maturation rate also differed between the sBM and sSL substrates, as observed through immunofluorescence staining of corneal cross-sections. The migrated epithelial cells on the sBM substrate formed multilayers and expressed tight junction protein ZO-1, and the limbal stem cell cytoskeleton marker K-14 expressed by the lower layer of migrated epithelial cells within 72 h (Fig. 3C). On the other hand, epithelial cells that migrated onto the sSL substrate formed a single layer and without tight junction detected (no expression of ZO-1). H&E staining further demonstrated multilayered epithelium formation on sBM and single layer epithelium on sSL. The results from the *ex vivo* cornea cultures indicate that sBM promotes faster epithelial cell migration and maturation as compared to sSL.

We tracked the epithelial cell maturation progress on the sBM layer over the 72 h time course via immunostaining of DAPI, K14 and ZO-1 (Fig. 4A). At 24 h the cells that migrated on to the sBM had larger cellular area of spread and a lower cell density, as observed using K14, ZO-1 and DAPI staining. These cells continued to proliferate, and by 48 h, sBM surface was covered with high cell density with smaller and polygonal morphology. At 72 h, epithelial cells formed a mature multilayered epithelium over the sBM implant, with smaller polygonal tight junctions in the lower layer (blue arrow indicated smaller polygonal tight junction), and flatter tight junctions on the cells closer to the top surface (white arrow indicated bigger tight junction), demonstrating a multilayered epithelium formation (Fig. 4A).

3.3. The synthetic stromal layer (sSL) modulates inflammatory gene expression and maintains corneal fibroblast phenotype following IL1-β stimulation

Next, we studied gene expression of corneal fibroblasts on both sBM and sSL substrates. The sSL layer contained biological ECM microparticles, which had been previously implicated to suppressed the inflammatory responses and reduced corneal scarring [33]. Gene expression of corneal fibroblasts (KERA, ALDH, and biglycan) as well as pro-inflammatory genes (IL6, IL8, and MMP9) were evaluated from rabbit corneal stromal fibroblasts that seeded on sBM, sSL, and tissue culture plastic (TCP) control. The KERA, ALDH and biglycan expressions of corneal fibroblasts seeded on both sBM and sSL were on a similar level compared to the TCP control, indicating that both sBM and sSL were able to maintain corneal fibroblast phenotype *in vitro*. Corneal fibroblasts on sBM expressed raised levels of IL6 and IL8 as compared to cells on TCP and sSL substrates (Fig 4Ba, 4Bb).

We further evaluated gene expression of corneal fibroblasts on the substrates with addition of IL1-β, which mimicked the initial inflammatory stimulation following *in vivo* corneal injury. Overall, IL-1β stimulation had no significant effects on keratocan and ALDH expressions, while increased biglycan expression in corneal fibroblasts cultured on TCP. Biglycan expression in cells on sBM and sSL substrates maintained similar level comparing to unstimulated cells on TCP control (Fig 4Bc). Corneal fibroblasts on TCP expressed significantly higher level of pro-inflammatory genes IL6, IL8 and MMP9 after IL-1β stimulation (Fig 4Bd). The cells on sBM showed upregulated IL8 expression while downregulated IL6 and MMP9 as compared to TCP control. The sSL substrates suppressed IL6, IL8 and MMP9 genes in corneal fibroblasts comparing to the stimulated cells on TCP. The gene expression results indicated that sSL containing ECM microparticles was able to maintain corneal fibroblast phenotype and downregulated inflammatory responses following IL-1β stimulation *in vitro*.

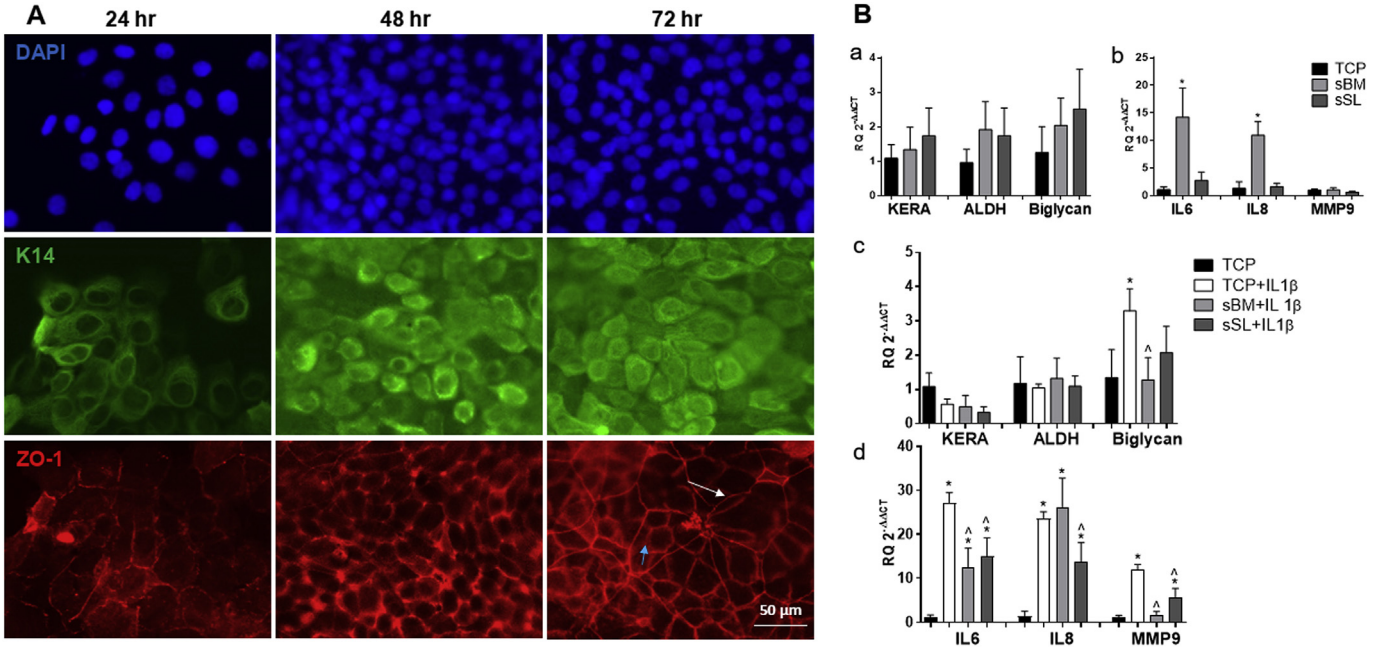

Fig. 4. Ex vivo epithelial cell maturation and in vitro corneal stromal fibroblast gene expression on sBM and sSL. A) The horizontal view of the epithelial cell migration and maturation on the sBM layer within 72 h. **B)** Gene expressions of corneal stromal fibroblasts on sBM and sSL material with and without IL-1β stimulation. Corneal fibroblasts maker genes and inflammatory genes on sBM and sSL layers under normal cell culture condition a) and b), and after stimulation with 20 ng/ml IL-1β for 24 h c) and d) (n = 5, *P < 0.05 Vs. TCP; ^P < 0.05 Vs. TCP + IL-1β).

3.4. Dual-layered cornea substitute enhances re-epithelialization and encourages corneal stromal regeneration

The dual-layered collagen vitrigel cornea substitute was implanted *in vivo* in a rabbit anterior lamellar keratoplasty model. We tracked the re-epithelialization process on day 7, 14, and 30 via fluorescein staining. Corneal epithelial cells migrated from the edge to the center of the implant as shown by the gross fluorescence staining picture at day 7. By day 14 post-surgery, over 95% of the dual-layered implant was covered by re-epithelialized cells. At 30 days post-surgery, the implanted cornea was fully re-epithelialized and remained clear (Fig. 5A, Supplemental Fig. 2A). OCT image revealed a distinctive boundary between host cornea and implanted vitrigel at day 7 post-surgery. By day 30, the boundary became indistinct, indicating host/implant integration (Fig. 5B). H&E staining of the full cornea receiving implanted material (Supplemental Fig. 2B) demonstrated complete re-epithelialization and restoration of corneal thickness compared to the negative control at day 30 post-surgery. Thickness of the central cornea (275.11 ± 23.75 μm) was not significantly different from the peripheral cornea (302.94 ± 24.59 μm). High magnified images showed migration of corneal stromal cells onto the implanted material. As a result, the implanted corneal substitute resembled nearly identical to the lamellae structure of the host tissue (Fig. 5C). Epithelial cells formed a multilayer structure on top of the implant, and positive immunofluorescent staining of K14 and p63 on the lower layers of the epithelial cells confirmed limbal stem cell migration onto the implanted material. ZO-1 staining showed that epithelial cells on the implant formed tight junctions within 30 days (Fig. 5D). In the central area of the implanted cornea, the epithelial cell expressed mature epithelial marker K3 and the stromal stained negative of myofibroblast marker α-SMA (Fig. 5D). Corneal epithelial cell marker K12, and integrin β4 also stained positive on the re-epithelialized cell layer. Trace positive of α-SMA marker was found at the edge of the implantation site, while inflammatory markers such as Thy1 and CD45 were undetected (Supplemental Fig. 2C). Taken together, these data demonstrated that the *in vivo* transplantation of the dual-layered collagen vitrigel corneal substitute via anterior lamellar keratoplasty was highly translational due to its ability to successfully restore structural, functional and biological properties of the damaged corneas.

4. Discussion

Due to the global donor tissue shortage and other factors such as tissue specificity and compatibility, the demand of finding alternative solutions is high. Current available corneal substitutes such as Boston Kpro or crosslinked human recombinant collagen are either lacking the abilities to achieve biointegration [5], or have limited mechanical integrity to bare interrupted suture techniques [34].

Previously, we created a collagen-based vitrigels incorporating β-cyclodextrin into collagen hydrogels to modulate collagen fibril self-assembly and alignment during vitrification [19]. Lamellar organization and fibrillar alignment in the vitrigels contribute to high optical transparency and mechanical robustness. However, migration of epithelial cells on to the implant material remains a challenge. The complete re-epithelialization on β-cyclodextrin/Collagen vitrigel takes as long as 30 days, delaying the healing of the cornea and implant/host tissue integration. Re-epithelialization is a critical first step in the corneal wound healing process following injuries or corneal transplantation. The delay in re-epithelialization or any disruption of this process would result in persistent corneal defects such as corneal haze or neovascularization, which eventually lead to an eventual transplant failure [35,36]. Re-epithelialization *in vivo* involves various confounding factors such as disruptions from eye lid movement, tear formation, immune cell recruitment and signaling [37]. To address this problem, Zhang et al. pre-seeded corneal epithelial cells on acellular porcine corneal matrix [38] before transplantation to accelerate the re-epithelialization process and to reduce neovascularization. However, preculturing cells on corneal substitute limits the transplant feasibility and significantly increased potential cost. Although the mechanical properties of decellularized cornea are more similar to native tissue, our dual-layered collagen vitrigel avoided complex decellular processing of whole tissue. Our solution demonstrated high optical transparency and displayed no to minimal neovascularization or haze formation when transplanted without preculturing epithelial cells.

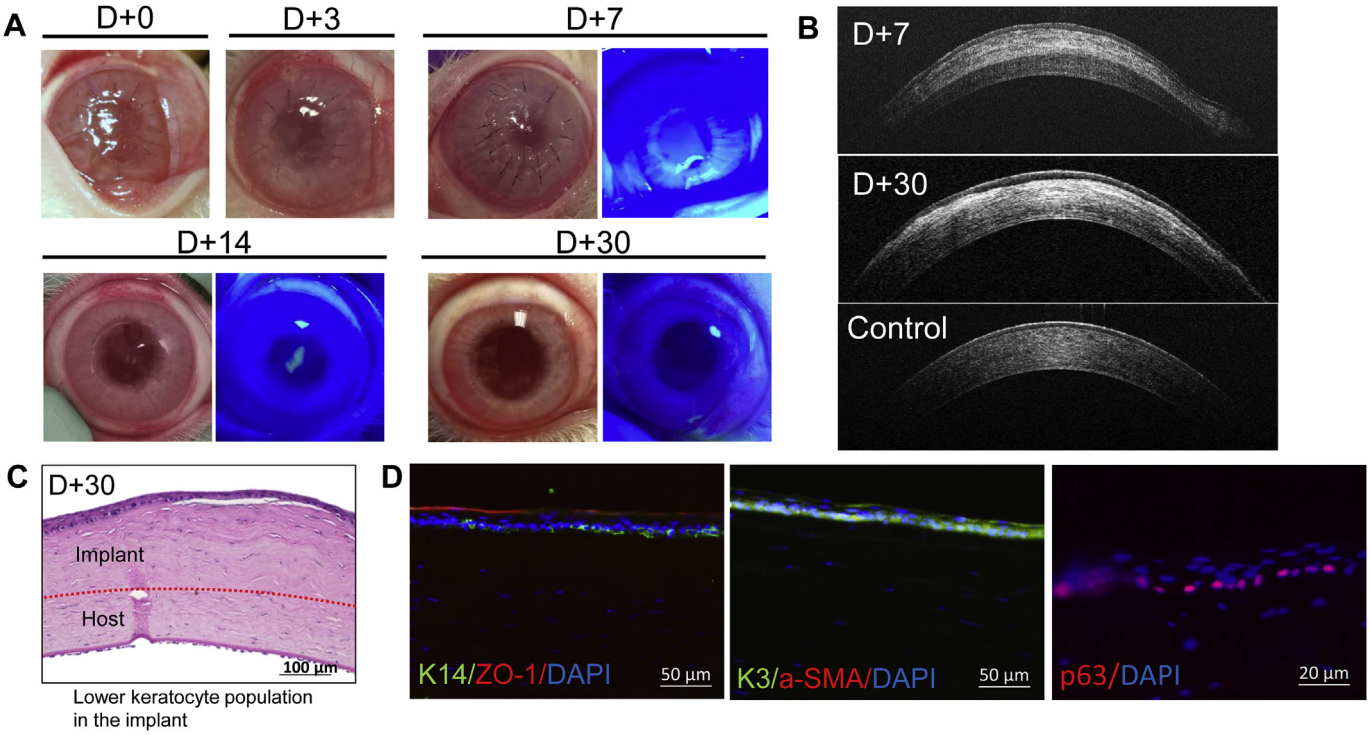

Fig. 5. In vivo surgical performance of the dual-layered collagen vitrigel corneal substitutes. A) Gross photos and fluorescein staining of rabbit eyes for *in vivo* evaluation on 0, 3, 7, 14, and 30 days post-surgery. B) OCT images on 7 and 30 days post-surgery demonstrating implant integration with the host tissue. C) H&E staining center corneal, and D) immunofluorescent staining of the central section showing epithelial cell multilayer formation and key marker expression on the implanted material.

We incorporated multiple improvements to the corneal substitute design. First, we used a complex biophysical process to add a thin layer of non-lamellar, amorphous, type I collagen sBM, which accelerated recovery of re-epithelialization both *in vitro* and *in vivo*. Collagen gelation by exposure to ammonia vapors in the thin layer limits the mobility of free collagen molecules and triple helices. The limitation of collagen molecule mobility generated non-lamellae structure after vitrification. This resulted in a homogenous network of sBM gel. Collagen fibril formation was observed only at interfaces, creating a gradient collagen matrix. Such gradient matrices have been previously reported where confined compression was the driving force [39]. This homogenous substrate with interfacial collagen fibrils allowed considerably faster epithelial cell migration *ex vivo* and *in vivo*. The epithelial cells formed multilayer on top of the sBM, and expressed limbal stem cell and epithelial cell key markers p63, K3, K12, and K14. Moreover, the major function of corneal epithelium is to serve as a physical and chemical barrier, and tight junction formation is one of the critical key markers of barrier formation [40]. The regenerated epithelium multilayer on sBM expressed tight junction protein ZO-1, suggesting that the migrated epithelial cells resemble the function of healthy cornea.

Second, we improved the mechanical strength and biological performance of synthetic stromal layer (sSL) by incorporating SIS ECM microparticles. Adding ECM particles into hydrogel system to form a composite scaffold is a well-accepted method to improve biomechanics of hydrogel materials [41]. Researchers in tissue engineering field investigated the use of ECM/hydrogel composite scaffolds, and showed that such scaffolds had superior mechanical and biological performance compared to traditional hydrogels [42–44]. In current study, the incorporation of ECM particles reinforced mechanical properties, and the vitrification of the ECM/collagen composite hydrogel clarified the final product during the controlled dehydration process. Vitrification process is the solidification of a liquid or a high water-content hydrogel [45]. We previously reported vitrification caused loss of inter- and intramolecular water in collagen hydrogel, and formed inter-molecular crosslinking [46]. This crosslinking contributed to the adhesive force between sBM and sSL, as well as the clarification of the final collagen vitrigels. Therefore, we are able to obtain an ECM-reinforced synthetic corneal stromal layer without compromising optical properties.

Corneal fibroblast activation is a critical factor in corneal tissue remodeling after injury or transplantation [47]. Following corneal injury *in vivo*, corneal epithelial cells secrete TGF-β and IL-1 cytokines, causing activation of quiescent corneal keratocytes and differentiation into corneal fibroblasts or myofibroblasts [48]. To preempt the wound healing issues arising from immune dysregulation, we used tissue-derived biological materials, which have been used for their pro-regenerative and immunoregulatory properties [27,49,50]. For example, OASIS®, a extracellular matrix product derived from porcine small intestinal submucosa (SIS), is approved by FDA for wound healing applications such as chronic leg ulcers [51]. In current study, we incorporated SIS-ECM microparticles in the synthetic stromal layer (sSL), achieving suppressed gene expressions of pro-inflammatory markers such as IL6, IL8 and MMP9. In our previous study [52], we reported collagen vitrigels with high density fibrillar structures and higher Young's modulus were beneficial to corneal keratocytes and fibroblasts. Synthetic BM substrate is a softer substrate with non-fibrillar collagen fibers. Therefore, immune markers of corneal fibroblasts expressed differently on the sBM from the sSL. The immunoregulatory potential from the ECM containing sSL might be an important factor contributing to the host/implant integration and the stromal regeneration. We validated this observation *in vivo* in rabbits, and found no sign of inflammation over the 30 days post-surgical time period.

In conclusion, we engineered a dual-layered biosynthetic corneal substitute, which provided clinically translational cornea-mimetic in physical properties including hight transparency and mechanical robustness, and biocompatibility with enhanced re-epithelialization and stromal regeneration. The sBM allowed rapid re-epithelialization and epithelial cell maturation , whereas the sSL modulated the inflammatory responses and provided mechanical support and suture

retention strength required for *in vivo* implantation. The dual-layered corneal substitute demonstrated minimal corneal scarring, and a promising host/implant integration within 30 days post-surgery, indicating its great potential as biosynthetic corneal substitute. Future studies will focus on improving the overall performance in translational applications. Longer time course animal experiment and more outcomes such as vision test will also be included.

Acknowledgements

This research was supported in part by the National Eye Institute grants R01EY029055, R01EY028666, Eyegenix LLC, and the Morton Goldberg Professorship. We would also like to acknowledge Scot C. Kuo (Director), Michael Delannoy (Associate Director) and Barbara Smith (EM & Advanced Fluorescence Microscopy Specialist) at the Microscopy Facility at Johns Hopkins School of Medicine, and EY001765 Wilmer Core Grant for Vision Research, and Mary Pease at Microscopy and Imaging Core Module.

Appendix A. Supplementary data

Supplementary data to this article can be found online at https://doi.org/10.1016/j.biomaterials.2020.119880.

Data availability

All datasets analyzed for this study are included in the manuscript and the supplementary files.

References

[1] J.P. Whitcher, M. Srinivasan, M.P. Upadhyay, Corneal blindness: a global perspective, Bull. World Health Organ. 79 (3) (2001) 214–221.
[2] P. Gain, R. Jullienne, Z. He, M. Aldossary, S. Acquart, F. Cognasse, et al., Global survey of corneal transplantation and eye banking, JAMA Ophthalmol 134 (2) (2016) 167–173.
[3] A.P. Patel, E.I. Wu, D.C. Ritterband, J.A. Seedor, Boston type 1 keratoprosthesis: the New York Eye and Ear experience, Eye 26 (3) (2012) 418–425.
[4] A.K. Riau, S.S. Venkatraman, C.H. Dohlman, J.S. Mehta, Surface modifications of the PMMA optic of a keratoprosthesis to improve biointegration, Cornea 36 (2017) S15–S25.
[5] R. Lee, Z. Khoueir, E. Tsikata, J. Chodosh, C.H. Dohlman, T.C. Chen, Long-term visual outcomes and complications of Boston keratoprosthesis type II implantation, Ophthalmology 124 (1) (2017) 27–35.
[6] B.D. Lawrence, J.K. Marchant, M.A. Pindrus, F.G. Omenetto, D.L. Kaplan, Silk film biomaterials for cornea tissue engineering, Biomaterials 30 (7) (2009) 1299–1308.
[7] C.R. McLaughlin, R.J.F. Tsai, M.A. Latorre, M. Griffith, Bioengineered corneas for transplantation and in vitro toxicology, Front Biosci-Landmrk 14 (2009) 3326–3337.
[8] P. Fagerholm, N. Lagali, W.B. Jacksson, M. Griffith, Biosynthetic corneas-2 Years after implantation in humans, Invest. Ophthalmol. Vis. Sci. 51 (13) (2010).
[9] M.M. Islam, O. Buznyk, J.C. Reddy, N. Pasyechnikova, E.I. Alarcon, S. Hayes, et al., Biomaterials-enabled cornea regeneration in patients at high risk for rejection of donor tissue transplantation, NPJ Regenerative medicine 3 (1) (2018) 2.
[10] T. Mimura, S. Amano, S. Yokoo, S. Uchida, S. Yamagami, T. Usui, et al., Tissue engineering of corneal stroma with rabbit fibroblast precursors and gelatin hydrogels, Mol. Vis. 14 (2008) 1819.
[11] R.A. Crabb, E.P. Chau, M.C. Evans, V.H. Barocas, A. Hubel, Biomechanical and microstructural characteristics of a collagen film-based corneal stroma equivalent, Tissue Eng. 12 (6) (2006) 1565–1575.
[12] E.S. Gil, S.H. Park, J. Marchant, F. Omenetto, D.L. Kaplan, Response of human corneal fibroblasts on silk film surface patterns, Macromol. Biosci. 10 (6) (2010) 664–673.
[13] R.M. Gouveia, E. González-Andrades, J.C. Cardona, C. González-Gallardo, A.M. Ionescu, I. Garzon, et al., Controlling the 3D architecture of Self-Lifting Autogenerated Tissue Equivalents (SLATEs) for optimized corneal graft composition and stability, Biomaterials 121 (2017) 205–219.
[14] S. Wang, C.E. Ghezzi, R. Gomes, R.E. Pollard, J.L. Funderburgh, D.L. Kaplan, In vitro 3D corneal tissue model with epithelium, stroma, and innervation, Biomaterials 112 (2017) 1–9.
[15] N. Saeidi, K.P. Karmelek, J.A. Paten, R. Zareian, E. DiMasi, J.W. Ruberti, Molecular crowding of collagen: a pathway to produce highly-organized collagenous structures, Biomaterials 33 (30) (2012) 7366–7374.
[16] P.D.S. Peixoto, A. Deniset-Besseau, M. Schmutz, A. Anglo, C. Illoul, M.-C. Schanne-Klein, et al., Achievement of cornea-like organizations in dense collagen I solutions: clues to the physico-chemistry of cornea morphogenesis, Soft Matter 9 (47) (2013) 11241–11248.
[17] A. Tidu, D. Ghoubay-Benallaoua, B. Lynch, B. Haye, C. Illoul, J.-M. Allain, et al., Development of human corneal epithelium on organized fibrillated transparent collagen matrices synthesized at high concentration, Acta Biomater. 22 (2015) 50–58.
[18] X. Calderon-Colon, Z.Y. Xia, J.L. Breidenich, D.G. Mulreany, Q.Y. Guo, O.M. Uy, et al., Structure and properties of collagen vitrigel membranes for ocular repair and regeneration applications, Biomaterials 33 (33) (2012) 8286–8295.
[19] S. Majumdar, X.K. Wang, S.D. Sommerfeld, J.J. Chae, E.N. Athanasopoulou, L.S. Shores, et al., Cyclodextrin modulated type I collagen self-assembly to engineer biomimetic cornea implants, Adv. Funct. Mater. 28 (41) (2018).
[20] H.S. Dua, J.A.P. Gomes, A. Singh, Corneal epithelial wound-healing, Br. J. Ophthalmol. 78 (5) (1994) 401–408.
[21] D.K. Pettit, T.A. Horbett, A.S. Hoffman, K.Y. Chan, Quantitation of rabbit corneal epithelial cell outgrowth on polymeric substrates in vitro, Invest. Ophthalmol. Vis. Sci. 31 (11) (1990) 2269–2277.
[22] R.M. Gouveia, G. Lepert, S. Gupta, R.R. Mohan, C. Paterson, C.J. Connon, Assessment of corneal substrate biomechanics and its effect on epithelial stem cell maintenance and differentiation, Nat. Commun. 10 (1) (2019) 1496.
[23] F. Kruse, A. Joussen, K. Rohrschneider, L. You, B. Sinn, J. Baumann, et al., Cryopreserved human amniotic membrane for ocular surface reconstruction, Graefe's Arch. Clin. Exp. Ophthalmol. 238 (1) (2000) 68–75.
[24] P.J. Adds, C.J. Hunt, J.K. Dart, Amniotic membrane grafts,"fresh" or frozen? A clinical and in vitro comparison, Br. J. Ophthalmol. 85 (8) (2001) 905–907.
[25] T.W. Gilbert, D.B. Stolz, F. Biancaniello, A. Simmons-Byrd, S.F. Badylak, Production and characterization of ECM powder: implications for tissue engineering applications, Biomaterials 26 (12) (2005) 1431–1435.
[26] S.F. Badylak, D.O. Freytes, T.W. Gilbert, Extracellular matrix as a biological scaffold material: structure and function, Acta Biomater. 5 (1) (2009) 1–13.
[27] H. Yin, Q. Lu, X. Wang, S. Majumdar, A.S. Jun, W.J. Stark, et al., Tissue-derived microparticles reduce inflammation and fibrosis in cornea wounds, Acta Biomater. 85 (2019) 192–202.
[28] V. Beachley, G. Ma, C. Papadimitriou, M. Gibson, M. Corvelli, J. Elisseeff, Extracellular matrix particle-glycosaminoglycan composite hydrogels for regenerative medicine applications, J. Biomed. Mater. Res. 106 (1) (2018) 147–159.
[29] S. Majumdar, X. Wang, S.D. Sommerfeld, J.J. Chae, E.N. Athanasopoulou, L.S. Shores, et al., Cyclodextrin modulated type I collagen self-assembly to engineer biomimetic cornea implants, Adv. Funct. Mater. 28 (41) (2018) 1804076.
[30] G. Scarcelli, R. Pineda, S.H. Yun, Brillouin optical microscopy for corneal biomechanics, Invest. Ophthalmol. Vis. Sci. 53 (1) (2012) 185–190.
[31] J.N. Webb, E. Langille, F. Hafezi, J.B. Randleman, G. Scarcelli, Biomechanical impact of localized corneal cross-linking beyond the irradiated treatment area, J. Refract. Surg. 35 (4) (2019) 253–260.
[32] T. Takezawa, K. Ozaki, A. Nitani, C. Takabayashi, T. Shimo-Oka, Collagen vitrigel: a novel scaffold that can facilitate a three-dimensional culture for reconstructing organoids, Cell Transplant. 13 (4) (2004) 463–473.
[33] H. Yin, Q. Lu, X. Wang, S. Majumdar, A.S. Jun, W.J. Stark, et al., Tissue-derived microparticles reduce inflammation and fibrosis in cornea wounds, Acta Biomater. 85 (2019) 192–202.
[34] I. Brunette, C.J. Roberts, F. Vidal, M. Harissi-Dagher, J. Lachaine, H. Sheardown, et al., Alternatives to eye bank native tissue for corneal stromal replacement, Prog. Retin. Eye Res. 59 (2017) 97–130.
[35] G.S. Polunin, V.V. Kourenkov, I.A. Makarov, E.G. Polunina, The corneal barrier function in myopic eyes after laser in situ keratomileusis and after photorefractive keratectomy in eyes with haze formation, J. Refract. Surg. 15 (2 Suppl) (1999) S221–S224.
[36] A.F. Drew, H.L. Schiman, K.W. Kombrinck, T.H. Bugge, J.L. Degen, A.H. Kaufman, Persistent corneal haze after excimer laser photokeratectomy in plasminogen-deficient mice, Invest. Ophthalmol. Vis. Sci. 41 (1) (2000) 67–72.
[37] M.A. Stepp, J.D. Zieske, V. Trinkaus-Randall, B.M. Kyne, S. Pal-Ghosh, G. Tadvalkar, et al., Wounding the cornea to learn how it heals, Exp. Eye Res. 121 (2014) 178–193.
[38] C. Zhang, L. Du, P. Sun, L. Shen, J. Zhu, K. Pang, et al., Construction of tissue-engineered full-thickness cornea substitute using limbal epithelial cell-like and corneal endothelial cell-like cells derived from human embryonic stem cells, Biomaterials 124 (2017) 180–194.
[39] K.M. Blum, T. Novak, L. Watkins, C.P. Neu, J.M. Wallace, Z.R. Bart, et al., Acellular and cellular high-density, collagen-fibril constructs with suprafibrillar organization, Biomater Sci-Uk 4 (4) (2016) 711–723.
[40] A.V. Ljubimov, M. Saghizadeh, Progress in corneal wound healing, Prog. Retin. Eye Res. 49 (2015) 17–45.
[41] J.M. Shapiro, M.L. Oyen, Hydrogel composite materials for tissue engineering scaffolds, JOM (J. Occup. Med.) 65 (4) (2013) 505–516.
[42] A. Shridhar, E. Gillies, B.G. Amsden, L.E. Flynn, Composite bioscaffolds incorporating decellularized ECM as a cell-instructive component within hydrogels as in vitro models and cell delivery systems Decellularized Scaffolds and Organogenesis, Springer, 2017, pp. 183–208.
[43] Q. Meng, Z. Man, L. Dai, H. Huang, X. Zhang, X. Hu, et al., A composite scaffold of MSC affinity peptide-modified demineralized bone matrix particles and chitosan hydrogel for cartilage regeneration, Sci. Rep. 5 (2015) 17802.
[44] V. Beachley, G. Ma, C. Papadimitriou, M. Gibson, M. Corvelli, J. Elisseeff, Extracellular matrix particle–glycosaminoglycan composite hydrogels for regenerative medicine applications, J. Biomed. Mater. Res. 106 (1) (2018) 147–159.
[45] G.M. Fahy, D. MacFarlane, C.A. Angell, H. Meryman, Vitrification as an approach to cryopreservation, Cryobiology 21 (4) (1984) 407–426.
[46] X. Calderón-Colón, Z. Xia, J.L. Breidenich, D.G. Mulreany, Q. Guo, O.M. Uy, et al.,

Structure and properties of collagen vitrigel membranes for ocular repair and regeneration applications, Biomaterials 33 (33) (2012) 8286–8295.
[47] M.E. Fini, Keratocyte and fibroblast phenotypes in the repairing cornea, Prog. Retin. Eye Res. 18 (4) (1999) 529–551.
[48] J.A. West-Mays, D.J. Dwivedi, The keratocyte: corneal stromal cell with variable repair phenotypes, Int. J. Biochem. Cell Biol. 38 (10) (2006) 1625–1631.
[49] K. Sadtler, S.D. Sommerfeld, M.T. Wolf, X.K. Wang, S. Majumdar, L. Chung, et al., Proteomic composition and immunomodulatory properties of urinary bladder matrix scaffolds in homeostasis and injury, Semin. Immunol. 29 (2017) 14–23.
[50] K. Lindberg, S.F. Badylak, Porcine small intestinal submucosa (SIS): a bioscaffold supporting in vitro primary human epidermal cell differentiation and synthesis of basement membrane proteins, Burns 27 (3) (2001) 254–266.
[51] E.N. Mostow, G.D. Haraway, M. Dalsing, J.P. Hodde, D. King, O.V.U.S. Group, Effectiveness of an extracellular matrix graft (OASIS Wound Matrix) in the treatment of chronic leg ulcers: a randomized clinical trial, J. Vasc. Surg. 41 (5) (2005) 837–843.
[52] Q. Guo, J.M. Phillip, S. Majumdar, P.-H. Wu, J. Chen, X. Calderón-Colón, et al., Modulation of keratocyte phenotype by collagen fibril nanoarchitecture in membranes for corneal repair, Biomaterials 34 (37) (2013) 9365–9372.